Electron microscopy of frozen water and aqueous solutions

by J. DUBOCHET, J. LEPAULT, R. FREEMAN, J. A. BERRIMAN *and* J.-C. HOMO, *European Molecular Biology Laboratory (EMBL), Postfach 10.2209, Meyerhofstr. 1, D-6900 Heidelberg, F.R.G.*

SUMMARY

Thin layers of pure water or aqueous solutions are frozen in the vitreous state or with the water phase in the form of hexagonal or cubic crystals, either by using a spray-freezing method or by spreading the liquid on alkylamine treated films. The specimens are observed in a conventional and in a scanning transmission electron microscope at temperatures down to 25 K. In general, the formation of crystals and segregation of solutes during freezing, devitrification and evaporation upon warming, take place as foreseen by previous X-ray, thermal, optical and electron microscopical studies. Electron beam damage appears in three forms. The devitrification of vitreous ice. The slow loss of material for the specimen at a rate of about one molecule of pure water for every sixty electrons. The bubbling in solutions of organic material for doses in the range of thousands of $e\ nm^{-2}$. We propose a possible model for the mechanism of beam damage in aqueous solutions.

The structural and thermal properties of pure frozen water important for electron microscopy are summarized in an appendix.

INTRODUCTION

Frozen aqueous solutions are the medium in which biological specimens are observed in cryo-electron microscopy. Much work has been done to characterize this medium (Luyet, 1965; MacKenzie, 1977), but unfortunately this study could not include homogeneous frozen dilute solutions as they separate into a phase of pure water in the form of hexagonal crystals (I_h) and a phase of concentrated solute. Much effort has also been put into the development of methods for preparing thin layers of frozen suspensions for observation in the electron microscope. In spite of some remarkable results (Fernandez-Moran, 1960; Taylor & Glaeser, 1976) the overall success has been limited probably by the difficulty of reproducibly obtaining good preparations and of manipulating frozen hydrated specimens. In order to contribute to the development of the methodology of observation of frozen hydrated specimens, we have started by studying simple model systems, namely pure water and diluted aqueous solutions. In this article we describe the simple prodecure we have adopted for manipulating and transferring frozen-hydrated specimens. We present also two methods for easy and reproducible preparation of very rapidly frozen thin layers of solutions. With these methods dilute solutions or even pure water can be frozen in the vitreous (I_v) state (Dubochet & McDowall, 1981). We report here our observations on the structure of pure ice and dilute frozen solutions and of the way they are

affected by the electron beam. This information is used in subsequent articles reporting on progress in the preparation and observation of frozen hydrated biological suspensions (Lepault *et al.*, 1982) and of cryosections (McDowall *et al.*, in preparation).

Because any understanding of the properties of frozen hydrated solutions is based on the knowledge of the properties of ice, we have summarized those which are important for electron microscopy in an Appendix.

MATERIAL
Electron microscopes

A conventional transmission electron microscope (CTEM) Philips 400 and a scanning transmission electron microscope (STEM) Vacuum Generators HB5 have been used for this work at an acceleration voltage of 80 or 100 kV. Under the working conditions of the Philips 400, residual water vapour leads to the condensation on the specimen of several tens or hundreds of nm of ice within minutes of its introduction. In order to prevent this effect we have built an additional cold trap formed by liquid nitrogen cooled blades placed just above and below the specimen, each with a 1 mm or 0·5 mm hole for the electron beam. This system reduces water condensation to the 10 nm range.

Cryo-specimen holders

The EM 400 is equipped with a cryo-specimen holder PW 6591/100, cooled by nitrogen gas flowing from a semi-closed reservoir of liquid nitrogen. Originally the temperature in the range down to 100 K could only be controlled by adjusting the pressure in the reservoir. In order to improve the temperature regulation of the specimen, we have stabilized the pressure in the reservoir to 101·33 kPa and regulated the flow by using a needle valve followed by a vacuum pump on the outlet from the cryo-holder. Several experiments, especially those requiring precise temperature control, have been made on a prototype of the cryo-transfer system for the EM 400 (Lichtenegger & Hax, 1980).

The cryo-specimen holder of the HB5 STEM has been described previously (Homo, 1980); it is cooled with nitrogen or helium gas and its temperature can be adjusted down to 25 K.

Unless otherwise stated, the specimens were mounted on carbon films on 200 mesh copper grids; in other cases collodion-carbon films or very thin carbon films mounted on perforated carbon films have also been used.

In the CTEM images were recorded on Kodak EM film 4489 with a speed of 0·5 μm^2 per electron and a saturation density of more than 7. Optical densities were measured from the micrographs with a Joyce Loebl 3CS microdensitometer.

METHODS
Transfer of frozen-hydrated specimens

A good transfer of frozen-hydrated specimens is achieved when external contamination is minimized and when the temperature of the specimen always remains below the devitrification temperature (T_v; approx. 130 K). These requirements are reasonably fulfilled by a very simple procedure we have used in all this work: the specimen, stored in liquid nitrogen, is mounted in the specimen holder under liquid nitrogen; this takes place in a box which eliminates most of the water condensation on the cold parts of the cryo-holder. Keeping the specimen under liquid nitrogen and the rest of the specimen holder protected from atmospheric humidity, it is brought to the airlock of the microscope then rapidly inserted. The time during which the specimen is exposed to the atmosphere is less than 5 s. Under these conditions, the amount of contaminating hexagonal ice (I_h) originating from the condensation of atmospheric humidity is generally small. The condensation of an I_v layer after the specimen is introduced into the microscope is more difficult to eliminate. This layer is easily recognizable because of its typical electron diffraction pattern, or because it leads to cubic ice (I_c) upon warming above T_v. Because the condensation generally takes place anisotropically, the I_v layer may produce a shadowing of superficial structures. This is illustrated in Fig. A1(c) of the Appendix. With the improved

anti-contamination device of the EM 400 and careful transfer, the deposition of I_v can be kept in the 10 nm range in the CTEM. It is even lower in the STEM.

The following test demonstrates that the temperature can be kept below I_v during the transfer. A characteristic pattern is produced by locally etching with the electron beam on an I_v layer condensed on a specimen; keeping the temperature as low as possible, the specimen holder is removed from the microscope and the grid from the holder; the grid is then reinserted as would be a new specimen; the characteristic I_v layer is conserved after this chain of operations.

Electron dose and mass-thickness measurements

Electron dose measurements in the CTEM are made from the optical density of the photographic film and with the electrometer used for the determination of the exposure time in the electron microscope. In the STEM, electron dose is calculated from the objective aperture current. In both cases the absolute calibration was made with a Faraday cage.

Methods for mass determination in the electron microscope are based on the measurement of the number of electrons scattered in the specimen (Zeitler & Bahr, 1962). To a first approximation, the number of scattering events in a thin layer of amorphous material is proportional to its mass thickness (Burge, 1973). The proportionality factor depends on the geometry of the optical system and, for a better approximation, on the nature of the material. The factor can be calculated on a theoretical basis. Using a 60 μm nominal objective aperture in the CTEM, corresponding to a semi-angle of $8 \cdot 3 \times 10^{-3}$ radian, the mass thickness of ice producing, on average, one scattering event per 80 kV electron is 190 mg m^{-2}. Other data covering most materials and conditions of image formation in the CTEM and STEM are given elsewhere (Eusemann *et al.*, 1982). In the CTEM mass determination is made using these data and measurements of optical densities on the micrographs. The system used in the STEM has been described elsewhere (Lamvik, 1978; Freeman & Leonard, 1981). The method can be applied directly to amplitude contrast images of amorphous specimens. For crystalline specimens care must be taken to average values over large areas and to avoid regions with bend contours.

The evaporation rate is determined from the difference in mass thickness measured from a series of micrographs recorded at close intervals or by recording the time variation of the current collected by the viewing screen.
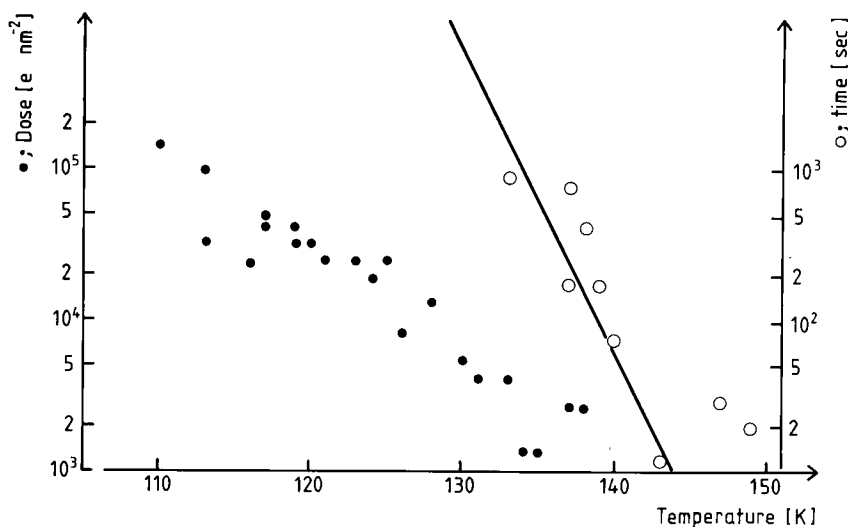
Temperature measurements

The three cryo-specimen holders used in this work are all equipped with a thermocouple, situated close to the specimen. Their calibration was frequently tested at room temperature and by immersion in liquid nitrogen ($77 \cdot 4$ K). The thermocouple of the STEM cryo-specimen holder was also calibrated with a carbon resistor located at the position of the specimen.

The temperature measure with the thermocouple is not *a priori* the real temperature of the specimen. Fortunately, ice itself can be used as a thermometer. This can be done by measuring the evaporation rate of ice (Talmon & Thomas, 1977, 1979). In Fig. 1 experimental values are plotted for the evaporation rate measured in the STEM and in the CTEM together with the theoretical curve deduced from the kinetic theory of gas, assuming an accommodation coefficient of 1 (Appendix). We have found that the devitrification temperature T_v also gives an accurate measurement of the local temperature on the specimen. For this experiment a layer of I_v is condensed on the specimen in the electron microscope. The temperature is then rapidly raised to some value between 130 and 144 K attainable to an accuracy of $\pm 2^\circ$ within less than 1 min. The transformation of vitreous into cubic ice is then best judged by electron diffraction when the second maximum of vitreous ice ($0 \cdot 214$ nm) is replaced by the 220 and 311 reflections of I_c at $0 \cdot 224$ nm and $0 \cdot 191$ nm respectively. In the favourable temperature range the same experiment was also performed with the other two cryo-specimen holders. Results are plotted in Fig. 2 together with the curve deduced from X-ray measurements (Dowell & Rinfret, 1960). It is also observed that the devitrification takes place almost simultaneously all over the grid and is independent of irradiation of adjacent areas by the electron beam.
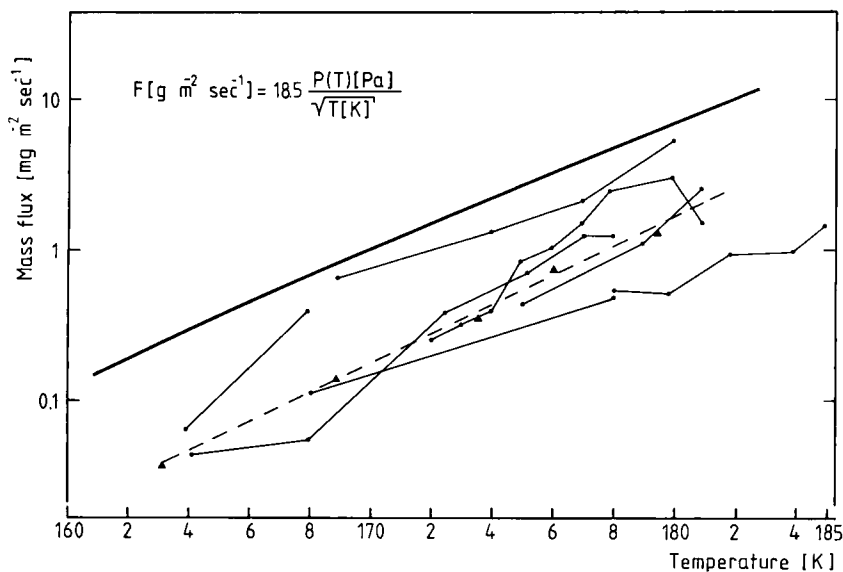
Fig. 1. Mass flux from the evaporation of ice at temperature T. The heavy line is calculated from the formula, which is deduced from the kinetic theory of gases assuming an accommodation coefficient of 1 (Appendix). Measurements made in the CTEM are marked by a dot. A light line joins those which have been obtained in the STEM. All measurements are made with electron doses for which beam damage is negligible.

Fig. 2. I_v–I_c transition as a function of the temperature. The right-hand side gives the time for transition with negligible electron irradiation. Open circles are experimental results obtained in the CTEM. The line is deduced from the measurements of Dowell & Rinfret (1960; Appendix). The left-hand side gives the electron dose required for the transition at a given temperature. Measurements have been made in the CTEM with 80 kV electrons.

From these observations we deduced that:

(1) The temperature of the specimen is uniform and is not significantly affected by heating due to the electron beam. This is in accordance with theoretical calculation and previous observations (Talmon & Thomas, 1978; Talmon *et al.*, 1979).

(2) The devitrification of I_v into I_c takes place within $\pm 2°$ of the temperature expected from X-ray studies (Dowell & Rinfret, 1960). The accuracy of this temperature measurement is nevertheless debatable because the glass transition temperature measured by thermal methods (Rasmussen & MacKenzie, 1971) is some 6° lower than indicated by our T_v measurements.

(3) The determination of the temperature of the specimen by the measurement of the evaporation rate of ice leads to $\pm 4°$ error due to the dispersion of the various results and to a systematic error of $-7°$. An accommodation coefficient smaller than 1 could account for the systematic error.

(4) The evaporation rate of I_c is not measurably different from the evaporation rate of I_h.

PREPARATION OF SPECIMENS

Specimens of frozen suspension must be thin and uniform over relatively large areas. It is difficult to obtain a thin layer of water because a high surface to volume ratio is being imposed on a liquid with high surface tension. Furthermore, the layer evaporates rapidly, thus making it more unstable. Consequently, most attempts lead to the preparation of specimens which are either dry or too thick. Several groups made considerable effort to develop suitable methods (MacKenzie & Luyet, 1962; Parsons *et al.*, 1974; Hayward *et al.*, 1978). We have used two methods, relying on the treatment of supporting films by low discharge (Dubochet *et al.*, 1982).

Thin film freezing

The method consists of forming a thin film of liquid by blotting away most of a drop from a *strongly hydrophilic* supporting film and immediately freezing it by immersion in cryogen. The exact conditions for removing the liquid with the blotting paper may seem critical. In practice, reproducible results can be obtained after a few trials. The grid carrying the drop is compressed by hand for about 1 s, between two double layers of dry filter paper (Whitman, Qualitative, 1). In order to minimize the time before freezing we use a simple mechanical device to project the grid from the blotting paper into the cryogen. The critical factor of the method is the surface property of the supporting film. Good preparations have frequently been obtained by making the film hydrophilic by glow discharge in air. We have obtained better and much more reproducible results on films treated by glow discharge at 100 Pa in alkylamine (e.g. pentyl-amine or tripropylamine, Fluka AG, Buchs, Switzerland). After this treatment the film is hydrophobic but becomes strongly hydrophilic when the solution is forced onto it. This suggests that the liquid layer is sandwiched between the carbon supporting film and the layer of molecules resulting from the glow discharge treatment in a similar way as in the oil sandwich method (Hayward *et al.*, 1978). Under the conditions described above, 80% of the grids are successfully prepared and have large areas, covered with a 50–300 nm thick layer of frozen solution.

Spray freezing

The principle of the method is to spray micro-droplets onto a hydrophilic supporting film and, after the droplets have spread, to freeze them before they evaporate. For good spreading, the film must be even more hydrophilic than for thin film freezing. In practice, sufficiently hydrophilic surfaces can be obtained after the glow discharge in air. The glow discharge apparatus should be clean and the film should be used immediately after treatment. We also believe that care should be taken to avoid oil vapour in the laboratory, and that freshly prepared films should be used. The hydrophilicity of films can be tested by spraying droplets of stain solution at room temperature. Circular droplets with well defined boundaries indicates that they have *not* spread correctly.

A schematic diagram of the spray freezing apparatus is shown in Fig. 3. The solution is sprayed from a commercially available nebulizer (Satagraph, Sanitaria GmbH, 7140 Ludwigs-burg, F.R.G.) pressurized with nitrogen gas at 222·93 kPa. The stream is limited by a 1 mm horizontal slit. An electron microscope grid supporting the hydrophilic film is held in a pair of tweezers, and is allowed to fall through the jet into the cryogen. The time between deposition of the droplet and freezing is determined by the geometry of the apparatus. Under the conditions
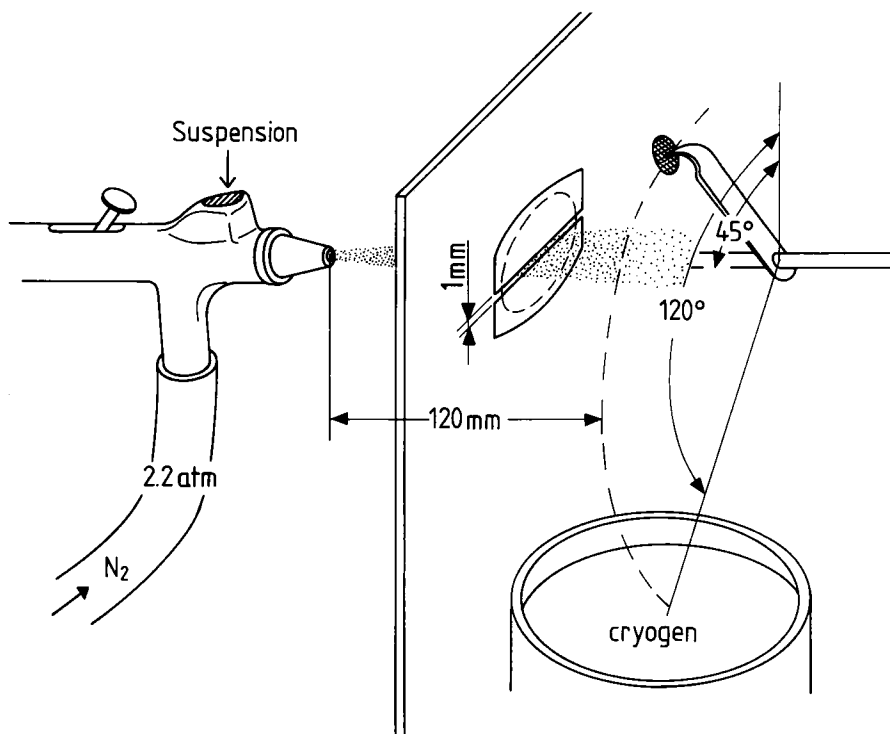
Fig. 3. Schematic of spray freezing apparatus.

shown in Fig. 3, 50% of the droplets have a volume smaller than 30 μm^3 and an adequate number of droplets are deposited on the film (one droplet per square on a 200 mesh grid); the time between deposition and freezing is 0·12 s and the speed when entering the cryogen is 2 m/s. Figure 4(a) shows a droplet frozen in boiling nitrogen 7×10^{-3} s after deposition and Fig. 4(b) shows one or more droplets frozen in nitrogen slush 0·12 s after deposition. The different aspect of these two micrographs is not only due to the different time span between deposition and freezing; the different wetting properties of the supporting films probably also plays a role.

From the results of this section and those on temperature and mass-thickness measurement, we conclude that samples of frozen hydrated specimens can reproducibly and relatively easily be prepared and transferred into the electron microscope. Beside a cold specimen stage, this requires no elaborate apparatus or special skill. In the microscope, the behaviour of water is close to what is expected from previous physical-chemical studies. This is, in particular, the case for the evaporation and the devitrification rate which both can serve as measurements of temperature.

STRUCTURE OF DILUTE FROZEN SOLUTIONS

The structure and physical properties of rapidly frozen solutions have been the subject of numerous studies, in particular we refer to Luyet (1965) and MacKenzie (1977) for a general description of the phenomena, to Luyet & Rasmussen (1967) for the study of polyvinylpyrrolidone (PVP), to Luyet & Rasmussen (1968) for the study of glycerol and sucrose solutions, and to Dowell *et al.* (1962) and MacKenzie & Luyet (1967) for the description of gelatine solutions. In general, it is found that increasing the cooling rate and raising the solute concentration both help in obtaining the vitreous state I_V. However, for dilute solutions, previous freezing methods have led to the segregation of the solutions into pure ice crystals and concentrated solute. Because the two methods we have described make it possible to prepare a very thin layer of liquid,
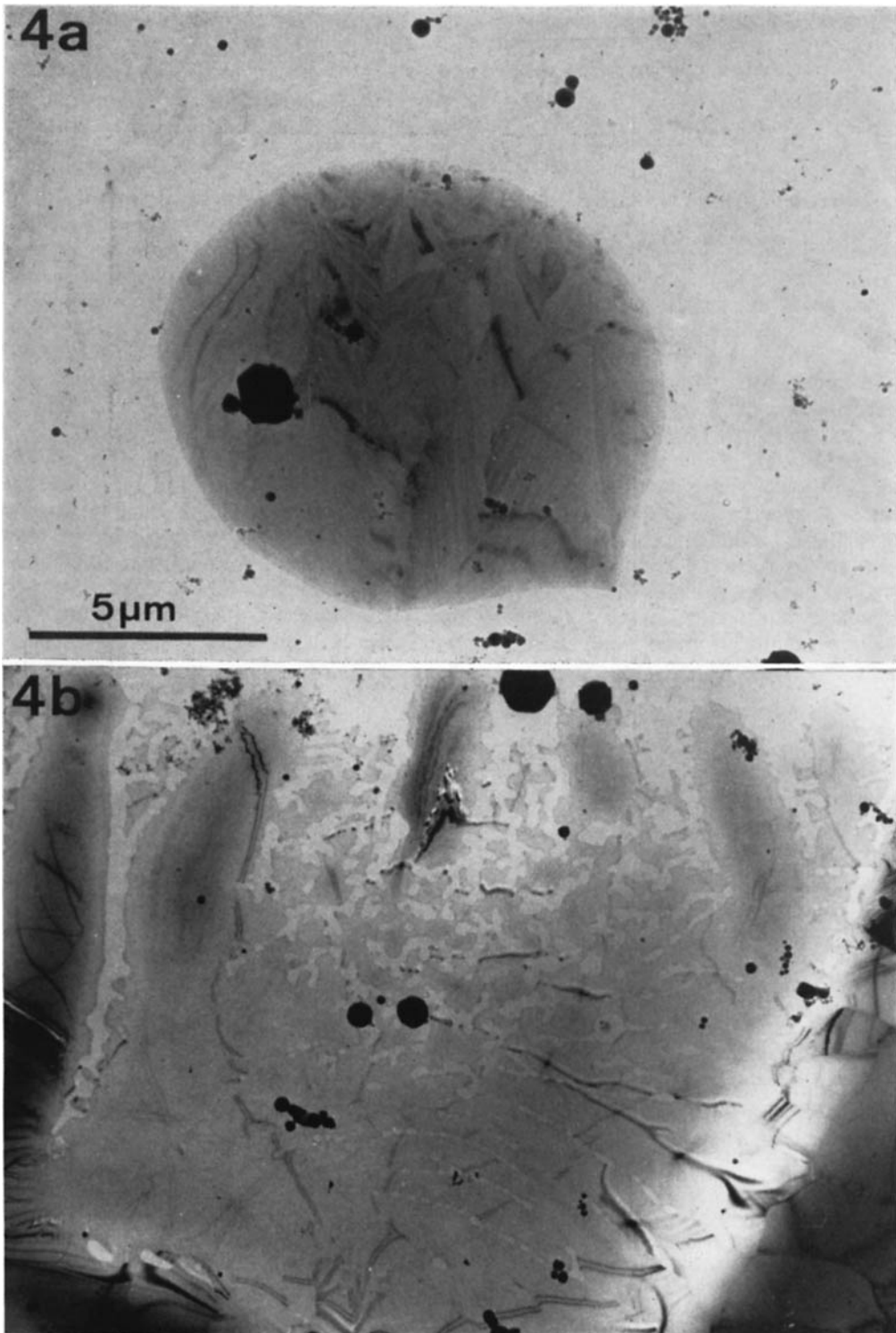
Fig. 4. Water prepared by spray freezing. (a) Droplet frozen in boiling nitrogen, 7×10^{-3} s after deposition. (b) Droplet(s) frozen in nitrogen slush 0·12 s after deposition. Magnification $\times 7000$.

we have been able to reach a higher freezing speed and therefore to observe dilute solutions and even pure water in the vitreous state. As test solutions, we have used sucrose, PVP, glycerol, gelatine and NaCl at concentrations of up to 20%.

Thin layers of pure water or of aqueous solutions can be frozen in the I_v, I_c or I_h form depending on the cryogen used and on the thickness of the layer. Vitrification is obtained with spray freezing (Dubochet & McDowall, 1981) and thin film freezing up to a thickness of 1 μm when samples are cooled in liquid propane or ethane at about 100 K. I_c crystals are formed when a thicker layer or a less efficient cryogen is used. This is the case for water layers up to 100 nm thick, frozen in nitrogen slush. These crystals are generally larger (μm) than those obtained by devitrification of I_v. When freezing is made in boiling liquid nitrogen, pure water is always in the I_h form. With solutions the I_c or I_v state can also be obtained depending on the solute, its concentration and the thickness of the layer. Among the various solutes we have studied, PVP was found to be the best cryoprotectant.

The typical appearance of frozen-dilute solutions is shown in Figs. 5–7. When frozen with water in the I_h form, dilute solutions have the same general aspect as a pure water layer in the I_h form (Appendix). Crystals are generally larger than 1 μm in the largest dimension. In most cases neighbouring crystals are oriented with their largest dimension roughly parallel. This is illustrated in Fig. 5, showing a frozen layer of a 3% PVP solution. When dilute solutions are cooled in the I_c form, they have the typical spherulite appearance shown in Fig. 6 for 10% sucrose droplets prepared by spray freezing. As its name implies, a vitrified solution shows no internal structure. The I_v state can nevertheless be unambiguously recognized on the direct image and by electron diffraction as shown in Fig. 7, the image of a droplet of frozen 10% sucrose solution. In this image only the periphery of the drop is amorphous. This is illustrated by the diffractogram of the region marked I_v where the ice layer is 60 nm thick. In the centre of the drop, ice is in the I_c form as indicated in the diffractogram of the marked region where the thickness is 230 nm.

*Partition of solute in frozen solutions*

In vitreous solutions the local concentration of the solute is probably unaffected by the freezing process. This is not the case when crystals are formed during freezing. While growing they expel molecules of the solute until the solution is divided into two phases: crystals of nearly pure water and a 'eutectic phase' formed by concentrated solute with a low concentration of unfreezable water. In the specimens described in this article, the 'eutectic phase' is characterized by the bubbling effect caused by the electron beam (see below) in the crystal interspaces. It is even more clearly visualized when the specimen is freeze-dried in the microscope. The 'eutectic phase' remains virtually unchanged after the evaporation of ice (MacKenzie, 1975). Evaporation of the aqueous regions originally in the vitreous state leads to a rearrangement of the solute molecules into a dense and characteristic network. The phenomenon is probably similar—but on much smaller scale—to the aggregations of dispersed biological particles during freeze-etching (Lepault & Dubochet, 1980). These phenomena are illustrated in Fig. 8, which shows a freeze-dried spray-frozen 10% sucrose droplet.

Our observations of the structure of frozen water and solutions underline the essential fact that only vitrified specimens show a structure similar to the liquid state. If vitrification is not

Fig. 5. (a) Square of a 400 mesh grid covered with a 300 nm thick layer of 3% PVP solution prepared by the alkylamine method and frozen in boiling nitrogen. Magnification × 1600. (b) Electron diffractogram of a 5 μm diameter area in (a).

Fig. 6. (a) Square of a 400 mesh grid covered with a 1800 to 460 nm thick layer of 10% sucrose solution prepared by the alkylamine amine method and frozen in boiling nitrogen. The micrograph has been recorded without objective aperture. Magnification × 1600. (b) Electron diffractogram of a 5 μm diameter area in (a).

Fig. 7. (a) Portion of a frozen 10% sucrose droplet prepared by spray freezing in boiling nitrogen. Magnification × 4100. (b) Electron diffractogram of the centre of the drop, marked I_c in (a). (c) Electron diffractogram of the border region of the drop, marked I_v in (a).
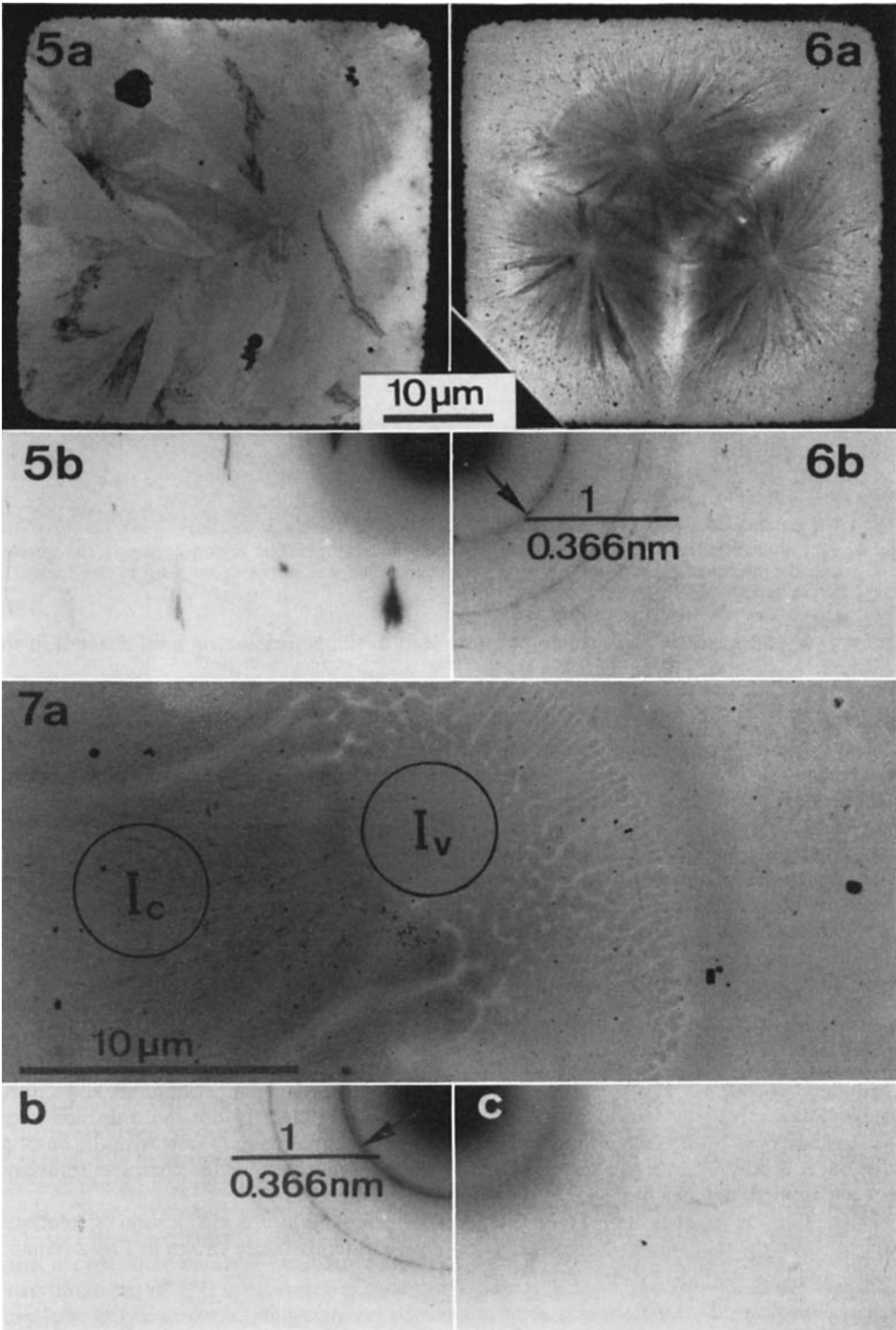
Figs. 5–7
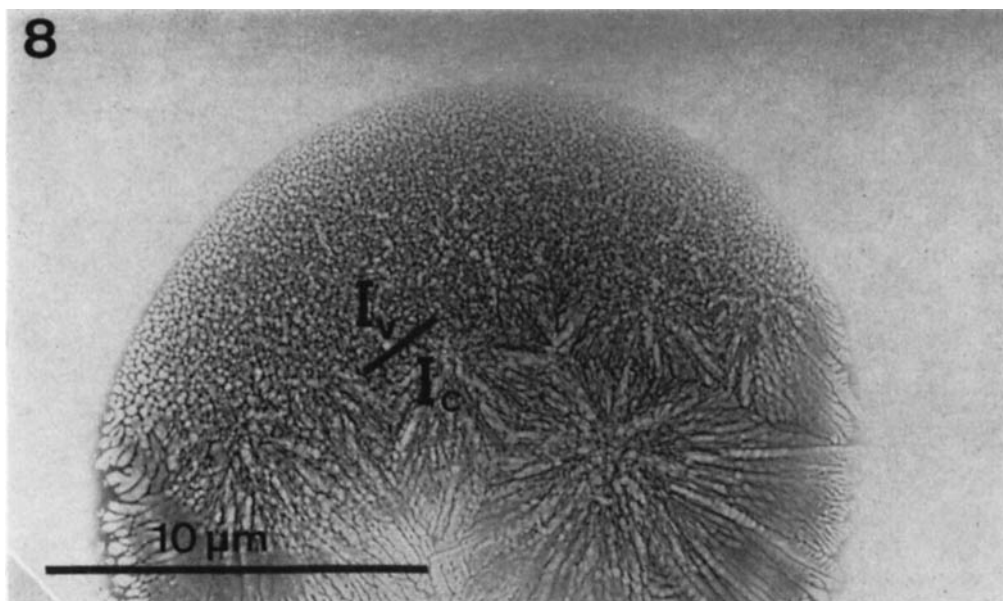
Fig. 8. 10% sucrose solution droplet freeze-dried in the microscope. The region I_v was in the vitreous state before the specimen was allowed to warm up whereas ice was in the cubic form in the region I_c. Magnification ×5000.

achieved, crystal formation and solute partition lead to fundamental structural changes in the specimen.

DAMAGE BY THE ELECTRON BEAM

For the electron microscopist used to working with very beam-sensitive organic material, the most remarkable property of water is its beam resistance. Indeed, when ice crystals are observed either directly or by electron diffraction, the only effect of the beam appears to be a slow mass loss but without change of the atomic structure of the residual material. Adding to the data already available on beam damage to frozen water (Glaeser & Taylor, 1978; Talmon *et al.*, 1979), we present here quantitative measurements of solutions observed in the CTEM and STEM between 25 K and room temperature for the three characteristic structural effects of beam damage, namely: devitrification, mass loss and bubbling. We have considered doses up to the 10^5 e nm^{-2} range but have concentrated on the conditions which are relevant to the observation of organic specimens; namely for doses below 10^4 e nm^{-2}.

Beam induced devitrification

In pure water the I_v–I_c transition can be triggered by the electron beam. As shown in Fig. 2, the dose needed for this transition increases with decreasing temperature. Below 110 K, beam induced mass loss causes the disappearance of the I_v layer before the transition takes place. As observed by electron diffraction, the transition does not seem to start with the onset of radiation, it is only when a half or two-thirds of the dose required for the complete transition has been applied, that the first sign of the transition becomes visible.

Despite having no quantitative measurements for beam induced devitrification of solutions, it appears that the relationship between electron dose and temperature shown in Fig. 2 remains roughly valid for aqueous solutions up to 20%.

Mass loss

Layers of water and aqueous solutions lose mass upon irradiation. As is the case at room temperature, there is a relatively large degree of variability on these phenomena. A factor of 2

between results of mass loss measured under similar conditions is not unusual. The basic characteristics of mass loss in pure water is illustrated in Fig. 9. It shows that, as a function of the electron dose, the mass loss is described by a straight line, the slope of which is independent of thickness. This is very different from results obtained on organic material at room temperature (for a summary, see: Dubochet, 1975, Fig. 3) where mass loss is described by a thickness dependent exponential curve. Figure 9 shows also that mass loss is independent of electron flux. There is, however, a marked difference between mass loss of vitreous ice and of crystalline hexagonal ice. Figure 10 shows that mass loss slowly decreases with decreasing temperature. It is more pronounced in aqueous solutions of organic material than in pure water.
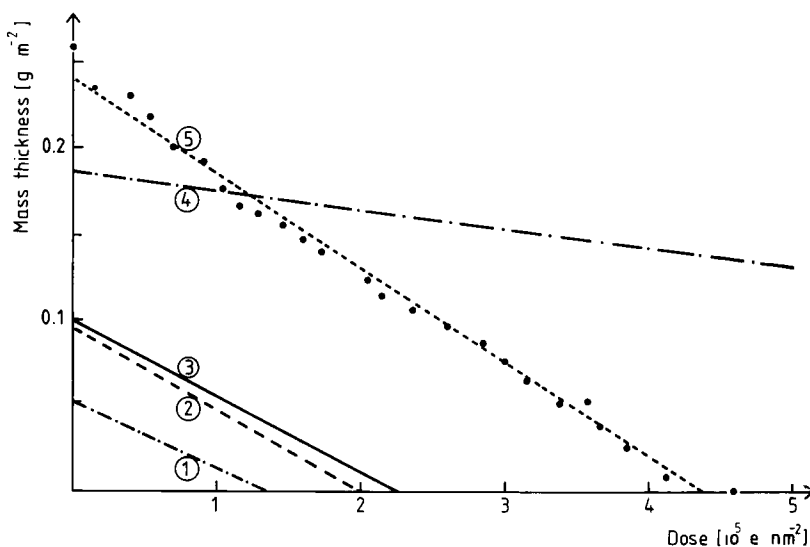

Fig. 9. Typical data for the mass loss of pure water as a function of the dose at 100 kV. The ordinate gives the mass thickness of the residual layer. (1) I_v layer irradiated at 110 K in the STEM with 15×10^3 e nm^{-2} per scan of 2 s and 10^{-11} A probe current. (2) I_v layer at 110 K, irradiated in the CTEM with a flux of 8×10^3 e nm^{-2} s^{-1}. (3) Same as (2) but with a flux of 10^3 e nm^{-2} s^{-1}. (4) I_h layer at 110 K irradiated in the CTEM with a flux of 2500 e nm^{-2} s^{-1}. (5) Same as (4) but at 150 K. The actual results from which this curve is drawn are also shown.

The following general features are deduced from the above and other similar data and are valid as long as there is not much bubbling (see below).

(1) Mass-loss is proportional to the dose but not to the thickness of the irradiated layer. For pure water in the I_v or I_c form at 110 K, at 100 kV approximately sixty electrons remove one water molecule. This is in agreement with the value of 120 found by Talmon *et al.* (1979).

(2) Mass-loss is independent of the electron flux and of the size of the irradiated surface. This is observed in the CTEM for fluxes of 10^3–8×10^3 e nm^{-2} s^{-1} and when the irradiation is periodically interrupted. This is confirmed by comparing results obtained in the CTEM with those of the STEM in which the flux is typically 10^5 times larger.

(3) Of the systems studied, aqueous solutions of organic material are the most susceptible to mass loss. Pure water in the I_v or I_c form is 2–5 times more resistant. Pure water in the I_h form is even more resistant by another factor of 2–5. However, when considering the apparent lower mass loss of I_h it is necessary to note that I_h layers deposited on one side of the supporting film have only one evaporating surface, whereas most measurements on I_v or I_c are made on layers which are probably condensed on both sides of the supporting film, thus offering two surfaces for evaporation.
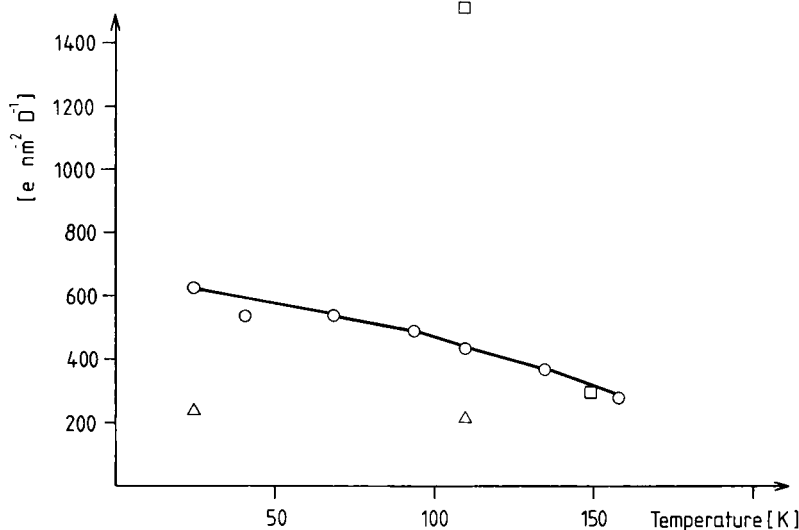
Fig. 10. Dose of 100 kV electrons required for removing 1 dalton of ice or of frozen solution as a function of the temperature. (○) Set of measurements obtained in the STEM on a 60 nm thick I_v layer (I_c at 158 K). (□) Average value (five measurements) for I_h in the CTEM. (△) Average value (three measurements. for a vitrified 10% sucrose solution in the STEM.

The above data suggest that the rate limiting step in mass loss is a *surface* phenomenon, namely, some kind of evaporation process. Radiolysis or a direct knock-on process would have a rate proportional to the *volume* of irradiated material. We also note that the dose of sixty electrons, which is required for removing one water molecule, is approximately the dose required to produce one inelastic scattering event per molecule (Eusemann *et al.*, 1981). The knock-on process, on the other hand, has a cross section which is about two orders of magnitude smaller (Unwin & Nuguruma, 1971; Dietrich *et al.*, 1978). Based on these considerations, it seems that beam induced mass loss in pure water is due to the removal of surface molecules, either by beam induced desorption or evaporation of radiolysis fragments. In the rest of the volume, irradiation has little structural effect.

Bubbling

The most obvious effect of beam damage to frozen solutions is bubbling. It is illustrated in Fig. 11 by a 10% vitreous solution of sucrose. A similar phenomenon has been observed by many cryo-electron microscopists and it has been described in particular by Talmon *et al.* (1979). Bubbling appears in dilute solutions of organic molecules following a dose of between 10^3 and 10^4 e nm^{-2}. Pure water or solutions of inorganic molecules also bubble (Unwin & Nuguruma, 1971) when the thickness of the layer is large and the electron flux high, but the dose required is roughly two orders of magnitude larger. Here we are only considering bubbling in aqueous solutions. Bubbling appears in all those which we have tested (sucrose, glycerol, PVP, gelatine) but not in NaCl solutions. It appears in I_v and for approximately the same dose in the interstitial volume between I_h crystals, but we have not observed it in solutions where ice is in the I_c form. Bubbling appears at a lower dose when the sample is observed at higher magnification. This suggests that the onset of the phenomenon is at an even lower dose, but on a scale which is too small to be recorded. With increasing dose the bubbles become larger. When the dose reaches to 10^4 or 10^5 e nm^{-2} range, mass loss becomes the predominant factor.

The dose required for bubbling increases with decreasing temperature. In 10% sucrose solutions it is 1500 e nm^{-2} at 130 K and 5000 e nm^{-2} at 25 K. According to E. Knapek (personal communication), it is around 5×10^4 e nm^{-2} at 4 K.
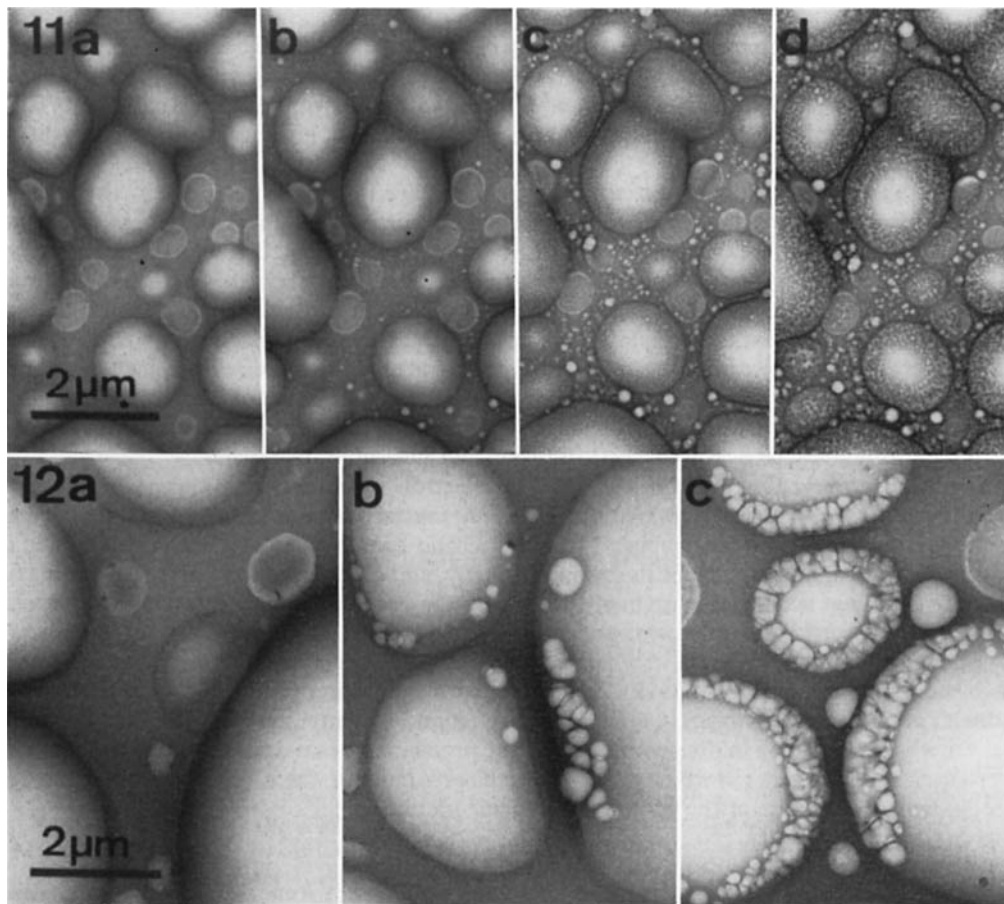
Fig. 11. Bubbling in a vitreous layer of 10% sucrose solution at 110 K. This series of micrographs shows the specimen having received a dose of 10^3, 2×10^3, 5×10^3 and 10^4 e nm^{-2} in figures a, b, c and d respectively. The flux during irradiation was 30 e nm^{-2} s^{-1}. The layer is mounted on a thin carbon film on a perforated carbon support. Magnification × 8600.

Fig. 12. 'Boiling' of a sucrose layer at 300 K. The specimen was irradiated with a total dose of 10^4 e nm^{-2} given with a flux of 500, 1000 and 3000 e nm^{-2} s^{-1} for a, b and c respectively. The supporting film is the same as in Fig. 11. Magnification × 8600.

Bubbling is only slightly dependent on flux. We have tested this point on sucrose solutions in the range between 10 and 1000 e nm^{-2} s^{-1} and when the irradiation is periodically interrupted. In this range, the dose for bubbling is not more than 50% larger at high flux than at low flux.

Bubbling is not strongly concentration dependent. It appears after a similar dose in I_v solutions or in the concentrated solute between I_h crystals. In pure sucrose—even sandwiched between two carbon layers to prevent contamination by condensed water—bubbling takes place for a dose only 30% smaller than in 10% vitreous solutions.

Comparison of beam damage at room temperature and at low temperature provides an understanding of the mechanism of bubbling. First, we note that beam induced mass loss which is drastically reduced at low temperature. Sucrose, for example, loses 50–60% of its mass according to a first order kinetic in which about two-thirds of the total loss is produced by a dose (D_e) of 1500–6000 e nm^{-2}. At 110 K, this dose is increased by nearly two orders of magnitude (Freeman *et al.*, 1980). Secondly, we frequently observed a phenomenon similar to bubbling but

appearing at room temperature. It is illustrated in Fig. 12 which shows a layer of sucrose irradiated with a dose of 10^4 e nm^{-2} applied at a flux of 500, 1000 and 3000 e nm^{-2} s^{-1} respectively. In the three cases the process of mass loss is virtually complete leaving only 40% of the initial mass. During the irradiation, the preparation seems to boil violently when irradiated at high flux, whereas the only effect observed in the bright-field CTEM at low flux is a uniform brightening of the image.

From the above observations we see that beam damage to sucrose happens in two phases. Molecular fragments are first formed by radiodecomposition of the material. These fragments then diffuse to the surface where they eventually evaporate. For sucrose, at room temperature and for high flux, the fragments cannot diffuse rapidly enough and begin to accumulate, building up pressure resulting in the effect shown in Fig. 12(c). Whereas the nature and the number of fragments is probably not much different when the irradiation takes place at low temperature, diffusion coefficients are drastically reduced. The fragments have therefore much more chance to accumulate. It is our hypothesis that bubbling is the consequence of this accumulation. A detailed understanding of the phenomenon will require a precise knowledge on the nature and chemistry of the fragments and on their diffusion and nucleation properties.

From our observations we conclude that, for electron irradiation conditions typically used in electron microscopy, the atomic structure of ice crystals is essentially stable, but the less stable vitreous ice can devitrify above 110 K. A second consequence of electron irradiation is mass loss due to a slow etching of the surface. Finally, and especially in the presence of organic material, bubbling takes place, probably caused by the accumulation of molecular fragments, unable to escape from the interior of the specimen.

As to the important question of whether the presence of water makes organic material more beam sensitive (Talmon *et al.*, 1979), our results with pure water, with pure organic material and with mixtures of both suggest, at first approximation, a negative answer. This does not mean that water is not involved in the process but, in the problem of beam damage, it appears that it is not so much organic material which suffers from the proximity of water, but water which is more readily damaged because of the presence of organic molecules.

REFERENCES

Burge, R.E. (1973) Mechanisms of contrast and image formation of biological specimens in the transmission electron microscope. *J. Microsc.* 98, 251.

Dietrich, I., Fox, F., Heick, H.G., Knapeck, E. & Weyl, R. (1978) Radiation damage due to knock-on processes on carbon foils cooled to liquid helium temperature. *Ultramicroscopy*, 3, 185.

Dowell, L.G., Moline, S.W. & Rinfret, A.P. (1962) A low-temperature X-ray diffraction study of ice structures formed in aqueous gelating gels. *Biochim. biophys. Acta*, 59, 158.

Dowell, L.G. & Rinfret, A.P. (1960) Low temperature forms of ice as studied by X-ray diffraction. *Nature*, 188, 1144.

Dubochet, J. (1975) Carbon loss during irradiation of T4 bacteriophages and *E. coli* bacteria in electron microscopes.. *J. Ultrastruct. Res.* 52, 276.

Dubochet, J., Groom, M. & Mueller-Neuteboom, S. (1982) Mounting of macromolecules for electron microscopy. In: *Advances in Optical and Electron Microscopy*, Vol. 8 (Ed. by V. E. Cosslett and R. Barer). Academic Press, London.

Dubochet, J. & McDowall, A.W. (1981) Vitrification of pure liquid water for electron microscopy. *J. Microsc.* 124, RP3.

Engel, A. (1978) Molecular weight determination by scanning transmission electron microscopy. *Ultramicroscopy*, 3, 273.

Eusemann, R., Rose, H. & Dubochet, J. (1982) Electron scattering in ice and organic materials. *J. Microsc.* 128, 239.

Fernandez-Moran, H. (1960) Low temperature preparation techniques for electron microscopy of biological specimens based on rapid freezing with liquid helium II. *Ann. N.Y. Acad. Sci.* 85, 689.

Freeman, R. & Leonard, K.R. (1981) Comparative mass measurements of biological macromolecules by transmission electron microscopy. *J. Microsc.* **122**, 275.

Freeman, R., Leonard, K.R. & Dubochet, J. (1980) The temperature dependence of beam damage to biological samples in the scanning transmission electron microscope. In: *Proceedings of the Seventh European Congress on Electron Microscopy* (Ed. by P. Brederoo and W. de Priester), Vol. 2, p. 640. Leiden.

Glaeser, R.M. & Taylor, K.A. (1978) Radiation damage relative to transmission electron microscopy of biological specimens at low temperature: a review. *J. Microsc.* **112**, 127.

Hayward, S.B., Grano, D.A., Glaeser, R.M. & Fisher, K.A. (1978) Molecular orientation of bacterio-rhodopsin within the purple membrane of halobacterium halobium. *Proc. nat. Acad. Sci. U.S.A.* **75**, 4320.

Homo, J.-C. (1980) Micro-cryostat for high resolution electron microscope specimen stage. In: *Proceedings of the Seventh European Congress on Electron Microscopy* (Ed. by P. Brederoo and G. Boom), Vol. 1, p. 92. Leiden.

Lamvik, M.K. (1978) Muscle thick filament mass measured by electron scattering. *J. molec. Biol.* **122**, 55.

Lepault, J., Booy, F.P. & Dubochet, J. (1982) *J. Microsc.* (submitted).

Lepault, J. & Dubochet, J. (1980) Freezing, fracturing and etching artefacts in particulate suspensions *J. Ultrastruct. Res.* **72**, 223.

Lichtenegger, S. & Hax, W.M.A. (1980) A cryo/transfer holder for TEM/STEM system. In: *Proceedings of the Seventh European Congress on Electron Microscopy* (Ed. by P. Brederoo and W. de Priester), Vol. 2, p. 652. Leiden.

Luyet, B.J. (1965) Phase transitions encountered in the rapid freezing of aqueous solutions. *Ann. N.Y. Acad. Sci.* **125**, 502.

Luyet, B.J. & Rasmussen, D.H. (1967) Study by differential thermal analysis of the temperatures of instability in rapidly cooled solutions of polyvinylpyrrolidone. *Biodynamica*, **10**, 137.

Luyet, B.J. & Rasmussen, D.H. (1968) Study by differential thermal analysis of the temperature instability of rapidly cooled solutions of glycerol, ethylene glycol, sucrose and glucose. *Biodynamica*, **10**, 167.

MacKenzie, A.P. (1975) Collapse during freeze-drying—qualitative and quantitative aspects. In: *Freeze-drying and Advanced Food Technology* (Ed. by S. A. Goldblith, L. Ray and W. N. Rothmayr), p. 277. Academic Press, London.

MacKenzie, A.P. (1977) Non equilibrium freezing behaviour of aqueous systems. *Phil. Trans. Roy. Soc.* B, **278**, 167.

MacKenzie, A.P. & Luyet, B.J. (1962) A collodion sandwich-film technique for the study of the growth of ice in very thin layers of aqueous solutions. In: *Proceedings of the Fifth International Congress for Electron Microscopy* (Ed. by S. S. Breise), Vol. 2, p. 2. Electron Microscopy, Philadelphia.

MacKenzie, A.P. & Luyet, B.J. (1967) Electron microscope study of recrystallization in rapidly frozen gelatin gels. *Biodynamica*, **10**, 95.

Parsons, D.F., Matricardi, V.R., Moretz, R.C. & Turner, J.N. (1974) Electron microscopy and diffraction of wet unstained and unfixed biological objects. *Adv. biol. med. Phys.* **15**, 161.

Rasmussen, D.H. & MacKenzie, A.P. (1971) The glass transition in amorphous water. Application of the measurements to problems arising in cryobiology. *J. Phys. Chem.* **75**, 967.

Talmon, Y., Davis, H.T., Scriver, L.E. & Thomas, E.L. (1979) Mass-loss and etching of frozen hydrated specimens. *J. Microsc.* **117**, 321.

Talmon, Y. & Thomas, E.L. (1977) Temperature rise and sublimation of water from thin frozen hydrated specimens in cold stage microscopy. In: *Scanning Electron Microscopy I* (Ed. by O. Johari), p. 265. IITRI, Chicago.

Talmon, Y. & Thomas, E.L. (1978) Electron beam heating temperature profiles in moderately thick cold stage STEM/SEM specimens. *J. Microsc.* **113**, 69.

Talmon, Y. & Thomas, E.L. (1979) Open system microthermometry—a technique for the measurement of local specimen temperature in the electron microscope. *J. Mater. Sci.* **14**, 1647.

Taylor, K.A. & Glaeser, R.M. (1976) Electron microscopy of frozen hydrated biological specimens. *J. Ultrastruct. Res.* **55**, 448.

Unwin, P.N.T. & Nuguruma, J.J. (1971) Transmission electron microscopy of ice. *J. appl. Phys.* **42**, 3640.

Zeitler, E. & Bahr, G.F. (1962) A photometric procedure for weight determination of submicroscopic particles by quantitative electron microscopy. *J. appl. Phys.* **33**, 847.

APPENDIX: STRUCTURE OF PURE ICE

This Appendix is a digest of the structural properties of ice which are the most important for cryo-electronmicroscopy. It is mainly based on the original reports from X-ray and electron microscopy studies, in particular by Blackman & Lisgarten (1957), Lonsdale (1958), Dowell & Rinfret (1960), Kumai (1968), and on our own observations. Exhaustive reviews are found in Hobbs (1974) and Franks (1972).

16

Ice can take three forms at normal or low pressure: the usual hexagonal ice (I_h), cubic ice (I_v) and vitreous (or amorphous) ice (I_v). These three forms are observed in cryo-electron microscopy. They can be distinguished by their general appearance and by electron diffraction. Figure A1 shows the typical aspect of the three forms of ice, together with their electron-diffractograms.

Hexagonal ice is obtained from cooled liquid water or by warming vitreous or cubic ice. The lattice parameters at 110 K are $a_0 = 0.449$ nm, $c_0 = 0.732$ nm, density: $\rho = 933$ kg m^{-3} and the linear thermal expansion coefficient is approximately 2×10^{-5}. The aspect of I_h crystals depends on their origin. They are always relatively large (μm) and are typically striated by bend contours when they originate from the freezing of liquid water. They appear as grains with more or less regular polygonal contours when they originate from the condensation of atmospheric water vapour on a cold specimen or in a cryogen. In that case their dimensions may be very small and they are frequently grouped in aggregates which are only partially in contact with the supporting film and are therefore easily displaced by the beam. Table A1 gives the position and the relative intensity of the main reflections seen by electron diffraction. The hexagonal form of heavy water has the same lattice parameters but a density of $\rho = 1040$ kg m^{-3}.

Table A1. Main reflections in the electron diffractogram of the various forms of ice at 110 K.

I_h	I_c	Vitreous	d (nm)	Intensity
100			0·389	Very strong
		First maximum	0·370	Very strong
002	111		0·366	Strong/very strong
101			0·343	Strong
102			0·266	Weak
110	220		0·224	Medium/medium
		Second maximum	0·214	
03			0·207	Medium
00			0·194	Very weak
112	311		0·191	Weak/weak
01			0·188	Very weak
02			0·172	Very weak

Cubic ice is obtained by deposition of water vapour in vacuum at a temperature between approximately 136 K and 170 K, by warming vitreous ice above the devitrification temperature T_v (c. 136 K) or by very rapid cooling of liquid water (Dubochet & McDowall, 1981). Once formed it is also stable below T_v. A small amount of I_h always appears to be present in the I_v phase as illustrated by the presence of the (100) form of I_h in Fig. A1(b). The lattice constant of I_c is 0·634 nm at 110 K. Its density is within 0·2% of the density of I_h. Cubic ice appears as a mosaic of small crystals with dimensions in the 0·1 μm range. Table A1 gives the position and relative intensity of the main reflections seen by electron diffraction. It should be noted that all reflections of I_c correspond to a relatively strong reflection of I_h. Consequently, the identification of I_c crystals from single crystal diffractogram is questionable.

Vitreous ice is obtained by the deposition in a vacuum of water vapour at temperatures below T_v or by rapid cooling of liquid water (Brueggeller & Mayer, 1980; Dubochet & McDowall, 1981). It has the same density as I_h and I_c. Vitreous ice appears as a smooth layer without internal

Fig. A1. Typical images and electron diffractograms of the three forms of ice. The direct images are all printed at the same magnification of × 10,000. (a) I_h obtained by rapid freezing of a thin water layer spread on a carbon film. The thickness of the layer shown on the micrograph is 50–80 nm. The diffractograms which are taken from other specimens show the (110) and (101) planes. (b) I_c obtained by warming a layer of I_v. The small contribution of the (100) form of I_h has been marked on the diffractogram (arrow). The I_c layer is approximately 70 nm thick. (c) I_v obtained by deposition of water vapour in the electron microscope on a film supporting polystyrene spheres. The layer is approximately 70 nm thick. The shadowing effect seen in this preparation demonstrates that the flux of water molecules hitting the specimen in the microscope was anisotropic.
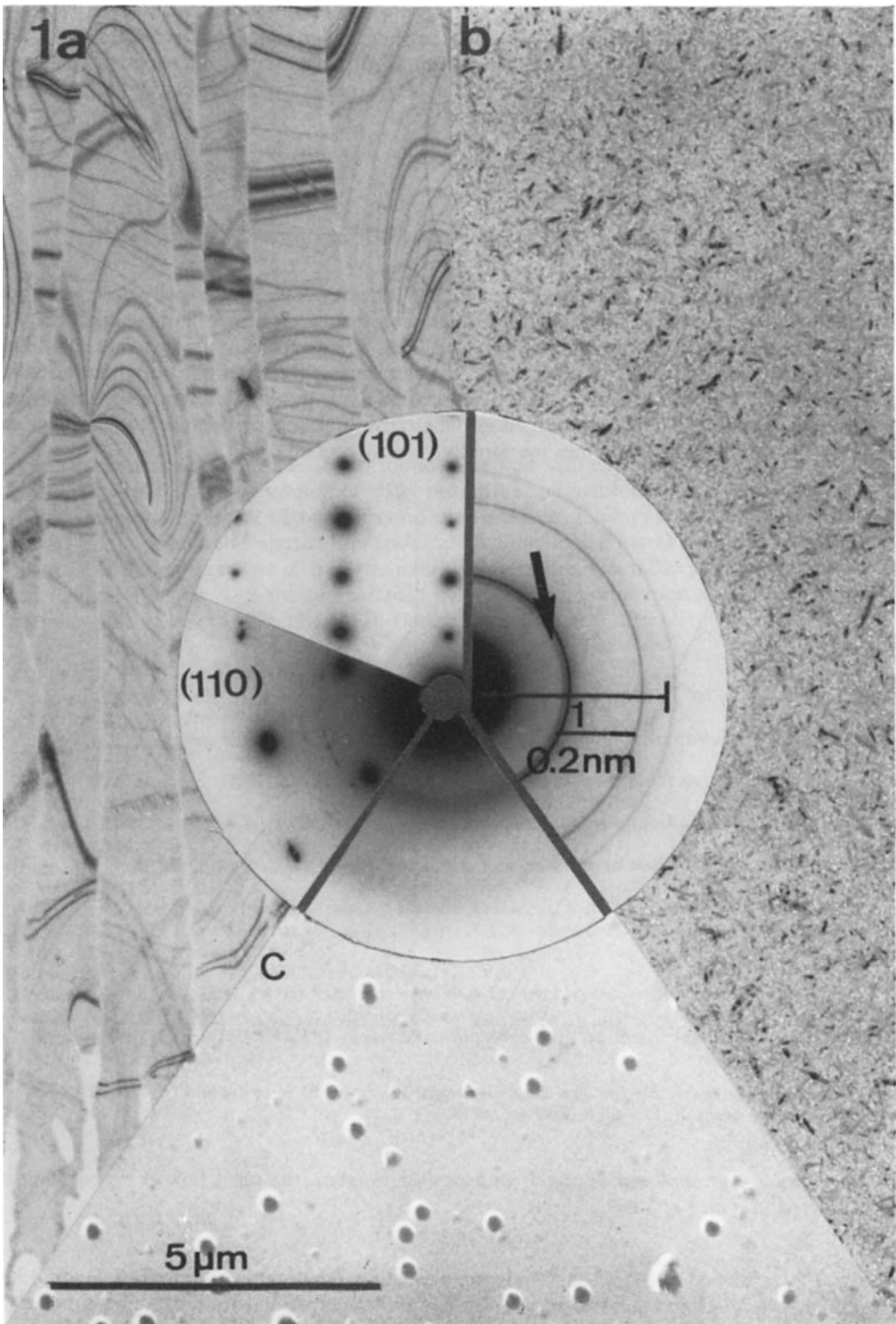
(101)

(110)

C

1

0.2nm

5 µm

Fig. A1

structure. The position of the two maxima seen by electron diffraction are given in Table A1. The half-width of the diffuse rings shows that the short-range order may extend up to 10 nm.

Phase transitions from I_v to I_c and from I_c to I_h are triggered by increased temperature. The time t (seconds) taken for the transition, rapidly decreases with increasing temperature T according to the equations (Dowell & Rinfret, 1960).

$$t = 1.22 \times 10^{30} \exp(-0.465T)$$

for the vitreous to I_c transition and

$$t = 1.55 \times 10^{14} \exp(-0.126T)$$

for the I_c to I_h transition.

These two equations are represented in Fig. A2. The devitrification is easily observed in the electron microscope. It should be noticed that this transformation is truly a phase transition and not a continuous extension of short-range order. This can be seen by the fact that the diffuse maxima of the vitreous state do not become sharper during the transition, eventually leading to the I_v pattern, but fade away while being replaced by the I_v pattern. Under normal conditions, the I_v to I_h transition cannot be observed in the electron microscope because it takes place at a temperature at which ice evaporates too rapidly.
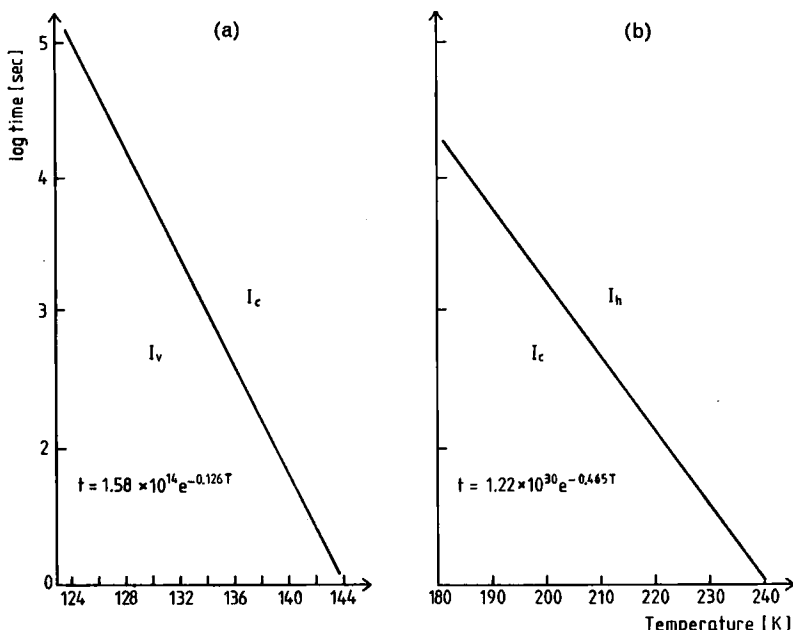

Fig. A2. Time t (seconds) required for the phase transition from (a) I_v to I_c, and (b) from I_c to I_h, as a function of temperature T (Dowell & Rinfret, 1960).

Evaporation and condensation of ice. In a perfect vacuum, the mass flux of evaporating ice F (expressed in g m^{-2} s^{-1}) is

$$F = 18.5\, P/\sqrt{T}$$

in which P (expressed in Pa) is the vapour pressure at the temperature T (Honig & Hook, 1960; Dushman, 1962). The factor becomes 2.47×10^3 if P is expressed in Torr. The curve $P(T)$ is given in Fig. A3. The $F(P,T)$ relation (represented in Fig. 1 of the preceding section) holds on the assumption that the accommodation coefficient (the probability that a molecule hitting
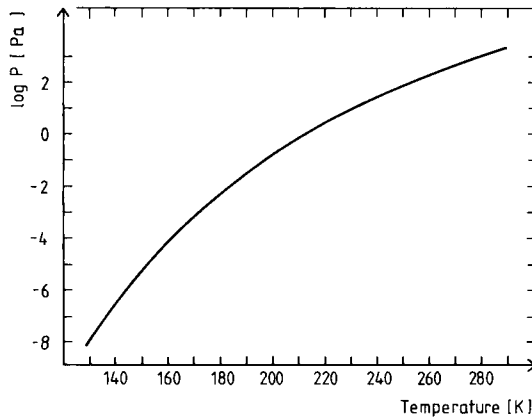
Fig. A3. Vapour pressure of water P (Pa) at temperature T (K) (Honig & Hook, 1960; Dushman, 1962).

the surface will stick to it) is 1. It was found to fit well with experimental measurements (Davy & Branton, 1970). The deposition of water onto the specimen follows the evaporation equation if P is the partial pressure of water around the specimen. It plays a significant role only if the partial pressure of water around the specimen is large or comparable to the vapour pressure of water at the temperature of the specimen. Furthermore, when the partial pressure of water is less than 10^{-6} Pa, and the temperature below 140 K, evaporation and condensation rates becomes so small as to be negligible in electron microscopical observations.

REFERENCES

Blackman, M. & Lisgarten (1957) The cubic and other structural forms of ice at low temperature and pressure. *Proc. Roy. Soc.* A, **239**, 93.

Bruegeller, P. & Mayer, E. (1980) Complete vitrification in pure liquid water and dilute aqueous solutions. *Nature*, **288**, 569.

Davy, J.D. & Branton, D. (1970) Subliming ice surfaces: freeze-etch electron microscopy. *Science*, **163**, 1216.

Dowell, L.G. & Rinfret, A.P. (1960) Low-temperature forms of ice as studied by X-ray diffraction. *Nature*, **188**, 1144.

Dubochet, J. & McDowall, A.W. (1981) Vitrification of pure liquid water for electron microscopy. *J. Microsc.* **124**, RP3.

Dushman, S. (1962) *Scientific Foundations of Vacuum Technique*, 2nd edn. John Wiley and Sons, New York.

Franks, F. (1972) The properties of ice. In: *Water, A Comprehensive Treatise* (Ed. by F. Franks), Vol. 1, p. 115. Plenum Press, New York.

Hobbs, P.V. (1974) *Ice Physics*. Clarendon Press, Oxford.

Honig, R.F. & Hook, H.O. (1960) Vapor pressure data for some common gases. *RCA Rev.* 21, 360.

Kumai, M.J. (1968) Hexagonal and cubic ice at low temperatures. *J. Glaciol.* **7**, 95.

Lonsdale, D.K. (1958) The structure of ice. *Proc. Roy. Soc.* A, **247**, 424.